Generalized Model Predictive Pulse Pattern Control Based on Small-Signal Modeling—Part 1: Algorithm

Tinus Dorfling, Hendrik du Toit Mouton, *Member, IEEE*, and Tobias Geyer, *Fellow, IEEE*

***Abstract*—A model predictive controller based on optimized pulse patterns is proposed that is suitable for higher-order linear systems, such as converters with LC filters. The controller manipulates the switching times of an optimized pulse pattern. The switching time modifications are approximated by the strengths of impulses, which are based on a small-signal linearization around the nominal switching instants. With these, the evolution of the state variables over the prediction horizon can be described by a set of linear differential equations. An objective function penalizes the predicted tracking error of the controlled variables, such as the converter currents, filter capacitor voltages, and grid currents, over a prediction horizon. Thanks to the use of impulse strengths, the underlying optimization problem is a convex quadratic program, which can be solved in real time to determine the switching time modifications of the pulse pattern to be applied by the controller.**

***Index Terms*—Model predictive control (MPC), optimized pulse patterns (OPPs), synchronous optimal pulse width modulation.**

I. Introduction

OPTIMIZED pulse patterns (OPPs) [1] are known for their superior harmonic performance. At low pulse numbers (i.e., at low switching frequency to fundamental frequency ratios), OPPs significantly outperform the well-known carried-based pulse-width modulation as well as state-of-the-art control techniques during steady-state conditions, see [2] and [3, Ch. 13.2]. This makes OPPs particularly beneficial for industrial power electronic systems that operate at low switching frequencies (such as medium-voltage drive systems). Due to the computationally demanding optimization problem underling OPPs, the switching angles of the pulse patterns are calculated offline over a range of modulation indices and pulse numbers; the switching angles are stored in lookup tables. During real-time operation of a converter system, the pulse pattern corresponding to the desired operating conditions is read-out from the lookup tables. It is important to realize that OPPs are (offline-calculated) *steady-state* switching sequences; the nominal pulse patterns are *only* optimal during steady-state conditions. During transients, OPPs are suboptimal and lead to a sluggish response; a high-bandwidth closed-loop controller is required to ensure a short response time.

However, designing a controller with a high dynamic performance for an OPP-modulated converter is a difficult task. Although control algorithms exist that address the control of first-order converter systems, the control of higher-order converter systems is a largely unexplored topic.

In this article, a new OPP-based model predictive control (MPC) method is proposed that achieves good performance during transients as well as during steady-state operation. The method

1) is applicable to any linear higher-order converter system with multiple state variables and integer switch positions,
2) regulates the system states along their optimal steady-state reference trajectories, and
3) achieves fast responses during transients.

The rest of this article is organized as follows. First, a review of existing control methods for OPPs is given in Section II. In Section III, a higher-order converter system is described, and it is shown how the steady-state trajectory of such a system can be determined. Section IV explains how the modifications of a pulse pattern are modeled by using the strengths of impulses. A model predictive controller is then derived in Section V. Finally, Section VI concludes this article.

The implementation and performance evaluation of the proposed control method are discussed in the second part of this article [4].

II. Review of Control Methods for OPPs

Unlike carried-based pulse-width modulation, OPPs lack a fixed-modulation interval and do not have regularly-spaced sampling instants at which the ripple component of certain converter quantities is zero. This implies that both the fundamental component and the ripple of the converter quantities are sampled. This results in classical linear controllers interpreting the ripple, which is a natural characteristic of the OPP, as an error. A linear controller will thus attempt to regulate the ripple to zero, resulting in suboptimal pulse patterns during the steady state. In order to prevent this, the bandwidth of the controller should be low so that it does not react to the ripple; consequently, the controller response becomes sluggish. Linear controllers are thus not a suitable choice for OPP-modulated converter systems that require a short response time.

Manuscript received May 26, 2021; revised November 14, 2021 and February 10, 2022; accepted April 8, 2022. Date of publication April 22, 2022; date of current version May 23, 2022. Recommended for publication by Associate Editor M. Perez. *(Corresponding author: Tinus Dorfling.)*

Tinus Dorfling and Hendrik du Toit Mouton are with the Department of Electrical and Electronic Engineer, Stellenbosch University, Stellenbosch 7599, South Africa (e-mail: martinusdorfling@protonmail.com; dtmouton@sun.ac.za).

Tobias Geyer is with the ABB System Drives, 5300 Turgi, Switzerland (e-mail: t.geyer@ieee.org).

Color versions of one or more figures in this article are available at https://doi.org/10.1109/TPEL.2022.3169113.

Digital Object Identifier 10.1109/TPEL.2022.3169113

A. Early Methods

As a first step away from a traditional linear controller for pulse patterns, a current trajectory controller was proposed in 1991 for electrical machines [5]. The method first determines the steady-state (stator) current trajectory that results from the pulse pattern. A deadbeat-type controller regulates the stator current along its steady-state trajectory by modifying the switching instants. In 2007, the method was adapted to control the stator flux instead of the stator current trajectory [6]. The advantage of tracking the stator flux trajectory is that the stator flux is independent of the leakage inductance of a machine. However, both methods require the fundamental component and ripple as separate quantities. Due to the fundamental component not being readily available when a converter is modulated by the pulse patterns, a dedicated observer is required [7].

B. Model Predictive Pulse Pattern Control

Recently, in 2012, the control problem underlying the OPPs was formulated in a model predictive control framework [8], giving rise to model predictive pulse pattern control (MP^{3}C) [9]. Arguably, MP^{3}C is the most established OPP-based method, as it is being used by ABB in their main medium-voltage drive system [10].

Consider a three-level converter (with a half dc-link voltage of $\frac{V_d}{2}$) that is modulated by a pulse pattern u and is connected to the stator of an induction machine. For simplicity, only a single phase is considered (the concept generalizes to all three phases). When neglecting the stator resistance, the stator flux ψ_s of an induction machine is simply the integral of the (input) stator voltage

$$\psi_s(t) = \psi_{s,0} + \frac{V_d}{2}\int_0^t u(\tau)\mathrm{d}\tau \tag{1}$$

where $\psi_{s,0}$ is the stator flux at the initial (sampling) instant. With (1) as the internal dynamic model of the predictive controller, the stator flux is predicted at the *end* of the prediction horizon T_p [that is, $\psi_s(T_p)$ is predicted]. Denote with n_{sw} the number of switching transitions that occur during the prediction horizon T_p. It is fairly straightforward to show that by modifying the ith switching transition of a pulse pattern by $\Delta t_i = t_i - t_i^*$, where t_i and t_i^* are the modified and nominal switching times, respectively, the modification in stator flux at the end of the horizon is

$$\Delta\psi_s(\Delta t_i) = -\frac{V_d}{2}\sum_{i=1}^{n_{\mathrm{sw}}}\Delta t_i \Delta u_i \tag{2}$$

where $\Delta u_i = u_i - u_{i-1} \in \{-1, 1\}$ is the change in switch position (also known as the so-called switching transitions).

Similar to the early trajectory-based methods, MP^{3}C regulates the stator flux ψ_s along its (optimal) steady-state trajectory ψ_s^*. Since the stator flux is simply the (scaled) integral of the pulse pattern, it is easy to derive the steady-state trajectory. Note that the MP^{3}C considers the instantaneous stator flux and, unlike the earlier methods, does not require the fundamental component and ripple to be separate quantities. Since an OPP is, per definition, optimal at steady-state operating conditions, the control algorithm makes no modifications to the pulse pattern in the steady state (assuming idealized conditions). This results in MP^{3}C having a dynamic response similar to the deadbeat-type controllers while having the superior harmonic performance of OPPs in the steady state, see [9] and [3, Ch. 13].

In [11], the MP^{3}C algorithm was extended so that carrier-based pulse-width modulated switching patterns can be generated online when operating at high pulse numbers and at low fundamental frequencies. Another control method, similar to the early trajectory-based methods and MP^{3}C, was proposed in [12].

As observed from (1), the internal dynamic model is an integrator. Examples of such loads are induction machines and grid-connected converters where the resistance can be neglected. However, this simple internal dynamic model is also a limitation of MP^{3}C; it is only applicable to (first-order) integrator systems. When considering higher-order systems, such as converters with LC filters, the internal dynamic model of MP^{3}C cannot capture the resonant behavior of the converter system. To account for this, MP^{3}C needs to be augmented by an additional damping term in its objective function [13], or an outer damping loop must be added [14]. Whilst these approaches might be effective during steady-state operation, the performance during large transients is rather poor. More specifically, to avoid exciting the filter resonance too strongly, large reference step changes should be filtered by a ramp-limiter, resulting in a sluggish step response. These limitations of MP^{3}C promote the need for a generalized OPP-based MPC scheme that is applicable to higher-order converter systems.

C. Methods for Higher-Order OPP-Modulated Systems

Although there exist control methods to address the higher-order OPP-modulated converter systems, these methods do have some characteristics that either make them impractical or limit their performance.

In [15], an MPC control problem is formulated with a continuous-time state-space model. The modifications to the switching instants are determined by solving a nonlinear program. However, sinusoidal references are used instead of the (optimal) steady-state trajectory resulting from the pulse pattern. This implies that the (natural) ripple from the pulse pattern is interpreted as an error and will thus be modified, which during steady-state conditions results in a suboptimal performance. The optimization problem, in its original nonlinear form, requires an optimization method to evaluate the matrix exponential at *every* iteration and, in addition, also requires a moderate amount of matrix multiplications; this results in a high computational burden. In order to simplify the optimization problem to a quadratic program (QP), the state variables are linearized around the nominal switching instants. However, the linearization requires that the three-phase voltage vectors have a fixed switching sequence. This implies that a switching transition in one phase cannot be shifted beyond a switching transition in another phase, thus imposing a major limitation. In combination with this limitation, the modifications to the switching transitions are also required to be very small due to the limited accuracy of the linearization. This results in very conservative constraints that

lead to a sluggish response during transients. Furthermore, at certain operating points, the linearized problem also significantly increases the harmonic distortion (see [15, Fig. 3]).

In [16], the MPC control problem is formulated using a discrete-time state-space model. Relative to the current sampling instant k, the controller predicts the system states at even-indexed switching instants (that is, at $k+2$, $k+4$, and so forth) and can manipulate the odd-indexed switching instants (that is, at $k+1$, $k+3$, and so forth). Note that the prediction instants are, therefore, irregularly spaced. The method introduces a nonlinear transformation of the decision variables (which are the odd-indexed switching instants), transforming the problem from a nonconvex optimization problem into a QP. As with [15], the state references are also sinusoidal and therefore suboptimal. Although the method assumes a fixed switching order, the response time is still modest. However, the method does make an assumption regarding the characteristics of the load: the total energy in the system stays constant during an unforced response (that is, when the input and grid voltage are zero), implying elements that dissipate power have to be ignored in the internal model.

Another generalized OPP-based controller is proposed in [17, Ch. 4]. The MPC problem is formulated in the discrete-time domain at regularly-spaced prediction instants. The core principle of the method is to transform the discrete-valued pulse pattern into a real-valued control signal that is easy to modify. This is achieved by averaging the pulse pattern between the discrete-time instants. Once the real-valued signal has been modified by solving a QP, a reverse transformation is required in order to retrieve the modified switching transitions. Unlike the methods in [15] and [16], this method uses the optimal steady-state trajectory that results from the pulse pattern as a reference. However, the method does have some limitations. The switching transitions are not allowed to move out of the sampling interval they are contained in; therefore restricting the degree by which the pulse pattern can be modified. Thus, in order to allow moderate modifications, the sampling interval is required to be relatively long. On the other hand, the averaging step introduces an error in the steady-state pulse pattern, which increases as the sampling interval is increased. This creates conflicting objectives. The reverse transformation itself requires an additional optimization problem to be solved: a linear program. Nonetheless, the method results in a decent response time and holds the most promise when compared to the methods of [15] and [16].

The controller proposed in Section V has none of the limitations of the aforementioned control methods, and is a natural generalization of MP^{3}C. Furthermore, the proposed controller is practically viable, as it has been implemented on a low-cost field-programmable gate array (see the second part of this article [4]) and can execute in real-time; none of the aforementioned methods have been verified to be practically feasible.

III. Converter System and Its Steady-State Trajectory

The formulation of the control algorithm in Section V is general enough so that any linear time-invariant system that is modulated with OPPs can be considered. This includes single-phase and multiphase converters, two-level and multilevel converters, inverters and rectifiers, and voltage-source and current-source converters. Such a power converter system with linear elements and integer inputs can be described by the continuous-time state-space representation as

$$\frac{\mathrm{d}\boldsymbol{x}(t)}{\mathrm{d}t} = \boldsymbol{F}\boldsymbol{x}(t) + \boldsymbol{G}\boldsymbol{u}_{abc}(t) + \boldsymbol{P}\boldsymbol{v}_g(t) \tag{3}$$

where $\boldsymbol{x} \in \mathbb{R}^{n_x}$ and $\boldsymbol{v}_g \in \mathbb{R}^{n_v}$ are the state and disturbance vectors, respectively, with $n_x \in \mathbb{N}^+$ and $n_v \in \mathbb{N}_0^+$. Note that it is assumed that the disturbance is known. The input vector $\boldsymbol{u}_{abc} = [u_a u_b u_c]^{\mathrm{T}} \in \mathbb{Z}^3$ is the three-phase switch position (this can easily be extended to the multiphase systems). Finally, $\boldsymbol{F}$, $\boldsymbol{G}$, and $\boldsymbol{P}$ are the state, input, and disturbance matrices, which characterize the system.

A. Case Study: Grid-Connected NPC Converter

As a case study, consider a three-level three-phase neutral-point-clamped (NPC) converter that is connected to the grid via an LC filter, as depicted in Fig. 1. The phase voltages are denoted by v_p, where $p \in \{a, b, c\}$ are the three phases. Assume that the dc-link capacitors have an infinite capacitance, and the neutral point N has no fluctuations, dividing the dc-link voltage V_d evenly across the dc-link capacitors.[1] Each phase leg can synthesize three voltage levels: $-\frac{V_d}{2}$, 0, and $\frac{V_d}{2}$. Thus, the output voltage for a particular phase is given by

$$v_p = \frac{V_d}{2} u_p$$

where $u_p \in \{-1, 0, 1\}$ represents the switch position of the particular phase.

The three-phase grid voltages are assumed to be symmetrical, and its phase voltages are shifted by 120° with respect to each other with a positive phase sequence.

B. State-Space Representation of a Grid-Connected NPC Converter

The three-phase converter current, capacitor voltage, and grid current are defined as $\boldsymbol{i}_{abc} = [i_a\ i_b\ i_c]^{\mathrm{T}}$, $\boldsymbol{v}_{c,abc} = [v_{c,a}\ v_{c,b}\ v_{c,c}]^{\mathrm{T}}$, and $\boldsymbol{i}_{g,abc} = [i_{g,a}\ i_{g,b}\ i_{g,c}]^{\mathrm{T}}$, respectively. These quantities are transformed into the stationary orthogonal reference frame with the Clarke transformation as

$$\boldsymbol{\xi}_{\alpha\beta} = \boldsymbol{K}\boldsymbol{\xi}_{abc}$$

which maps any variable $\boldsymbol{\xi}_{abc} = [\xi_a\ \xi_b\ \xi_c]^{\mathrm{T}}$ in the abc-plane to the 2-D vector $\boldsymbol{\xi}_{\alpha\beta} = [\xi_\alpha\ \xi_\beta]^{\mathrm{T}}$ in the $\alpha\beta$-plane via the transformation matrix

$$\boldsymbol{K} = \frac{2}{3}\begin{bmatrix} 1 & -\frac{1}{2} & -\frac{1}{2} \\ 0 & \frac{\sqrt{3}}{2} & -\frac{\sqrt{3}}{2} \end{bmatrix}.$$

Based on this, the state vector is defined as

$$\boldsymbol{x} = \begin{bmatrix} i_\alpha & i_\beta & i_{g,\alpha} & i_{g,\beta} & v_{c,\alpha} & v_{c,\beta} \end{bmatrix}^{\mathrm{T}}$$

[1] To address the balancing of the neutral-point potential, the methods proposed in [18] and [19] can be incorporated in the control algorithm.

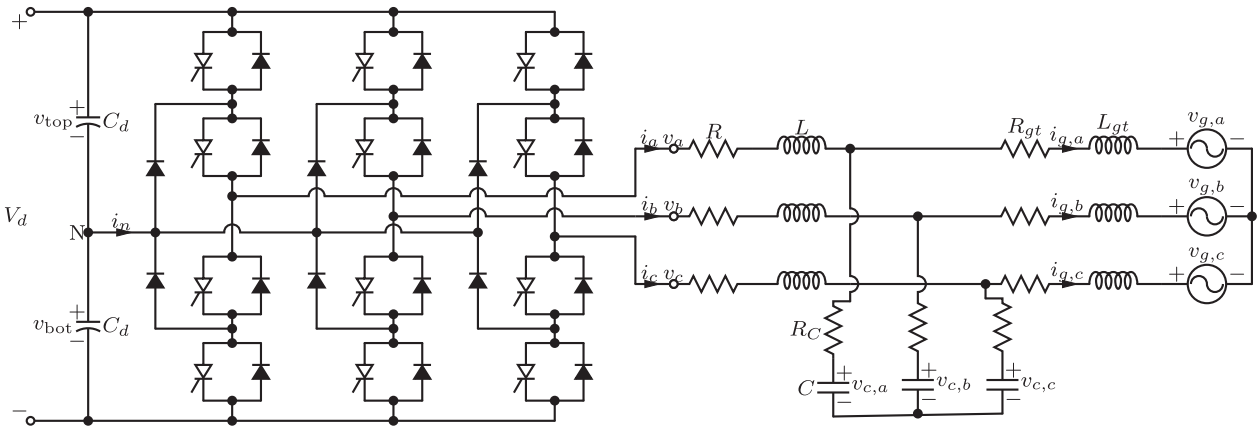

Fig. 1. Grid-connected NPC converter with an LC filter. The resistances and inductances of the grid and transformer are lumped together as $R_{gt} = R_g + R_t$ and $L_{gt} = L_g + L_t$, respectively. Note that the resistors represent the equivalent series resistances of the filter inductor and capacitor, as well as the winding resistance of the transformer.

and the converter system is described in a continuous-time state-space form using (3). The grid voltage is defined in the stationary orthogonal reference frame as

$$\boldsymbol{v}_g(t) = \begin{bmatrix} v_{g,\alpha}(t) \\ v_{g,\beta}(t) \end{bmatrix} = \sqrt{\frac{2}{3}} V_g \begin{bmatrix} \sin(\omega_1 t) \\ -\cos(\omega_1 t) \end{bmatrix}$$

where V_g is the root-mean-square line-to-line grid voltage, and $\omega_1 = 2\pi f_1$ is the fundamental angular frequency. The state-space matrices are shown in the Appendix A. The grid voltage $\boldsymbol{v}_g$ is treated as a known disturbance. Note that the input $\boldsymbol{u}_{abc}$ is given in the three-phase abc frame, whereas the state vector $\boldsymbol{x}$ and the disturbance vector $\boldsymbol{v}_g$ are given in the stationary orthogonal $\alpha\beta$ reference frame.

C. Steady-State Trajectory of a Converter System Modulated by OPPs

The following method is a modification to the method proposed in [20].

It can be shown from (3) that the steady-state trajectory resulting from the nominal pulse pattern $\boldsymbol{u}^*_{abc}$ at time $t \in [0, T_1]$, where T_1 is the fundamental period, is

$$\boldsymbol{x}^*(t) = \boldsymbol{e}^{\boldsymbol{F}t}\boldsymbol{x}^*_0 + \int_0^t \boldsymbol{e}^{\boldsymbol{F}(t-\tau)}\boldsymbol{G}\boldsymbol{u}^*_{abc}(\tau)\mathrm{d}\tau + \int_0^t \boldsymbol{e}^{\boldsymbol{F}(t-\tau)}\boldsymbol{P}\boldsymbol{v}_g(\tau)\mathrm{d}\tau \quad (4)$$

where $\boldsymbol{x}^*_0$ is the initial steady-state value at the start of the fundamental period T_1. In order to calculate the steady-state trajectory over a fundamental period, the initial steady-state value $\boldsymbol{x}^*_0$ first needs to be calculated. Thanks to linearity, the principle of superposition can be used to calculate the effect of the pulse pattern and grid voltage separately as

$$\boldsymbol{x}^*(t) = \boldsymbol{x}^*_{\text{OPP}}(t) + \boldsymbol{x}^*_g(t) \quad (5)$$

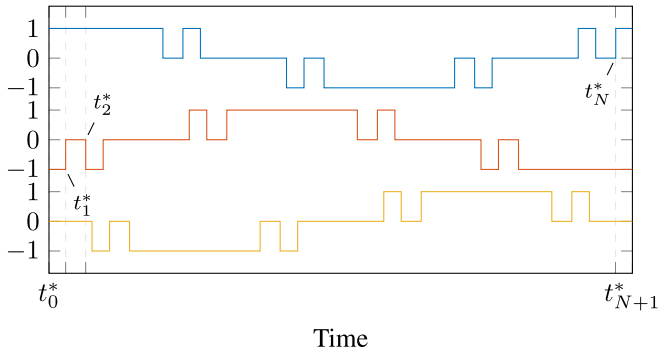

Fig. 2. Three-phase nominal pulse pattern $\boldsymbol{u}^*_{abc}$. The pulse number is $d = 3$, and there are a total of $N = 36$ switching transitions across all three phases.

where

$$\boldsymbol{x}^*_{\text{OPP}}(t) = \boldsymbol{e}^{\boldsymbol{F}t}\boldsymbol{x}^*_{\text{OPP},0} + \int_0^t \boldsymbol{e}^{\boldsymbol{F}(t-\tau)}\boldsymbol{G}\boldsymbol{u}^*_{abc}(\tau)\mathrm{d}\tau. \quad (6)$$

For now, the grid is ignored and assumed to be short-circuited. Consider the (three-phase) nominal pulse pattern in Fig. 2, which has $N = 12d$ switching transitions over the fundamental period T_1 (where d is the pulse number). Denote with t_i^* the (three-phase) nominal switching times, where $i = 0, 1, \ldots, N+1$. The switching times $t_0^* = 0$ and $t_{N+1}^* = T_1$ are introduced to take the boundaries into account. Due to periodicity, it always holds that

$$\boldsymbol{x}^*_{\text{OPP}}(0) = \boldsymbol{x}^*_{\text{OPP}}(T_1) \quad (7)$$

in steady-state conditions; this fact can be used to calculate $\boldsymbol{x}^*_{\text{OPP},0}$. It is easy to see from (6) that

$$\boldsymbol{x}^*_{\text{OPP}}(0) = \mathbf{I}_{n_x}\boldsymbol{x}^*_{\text{OPP},0} \quad (8)$$

where $\mathbf{I}_{n_x}$ is the identity matrix of dimensions n_x. To calculate $\boldsymbol{x}^*_{\text{OPP}}(T_1)$, note that the three-phase pulse pattern is constant between the switching transitions. This leads to the integral

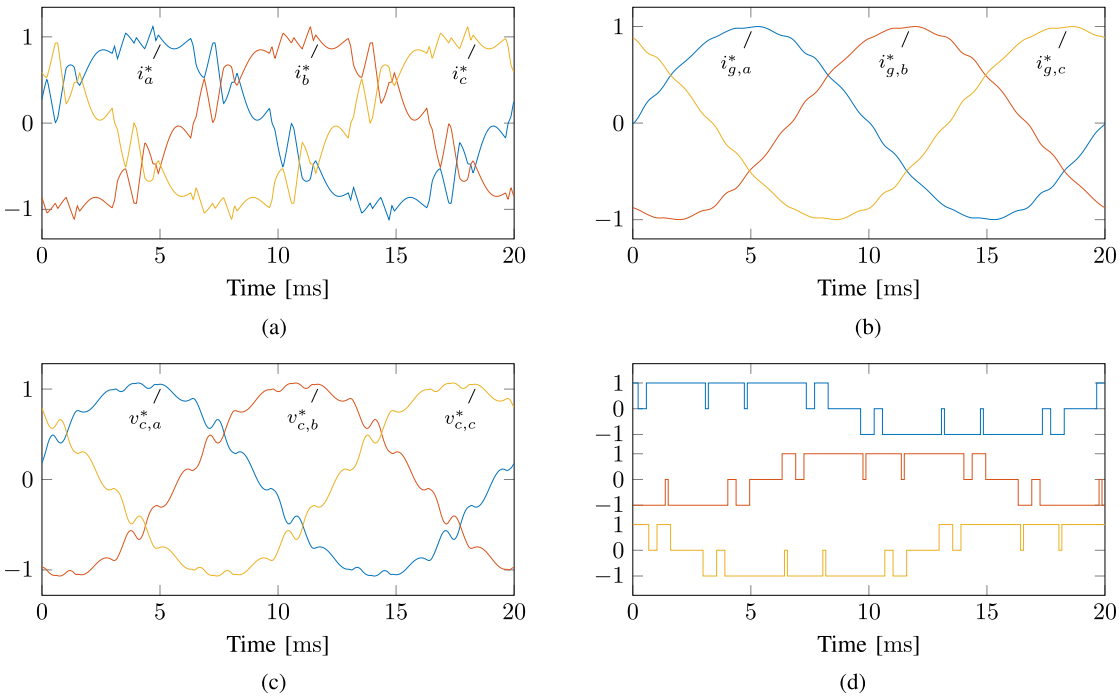

Fig. 3. Steady-state trajectory (in p.u.) of the converter system resulting from the nominal pulse pattern $\boldsymbol{u}_{abc}^*$ (including the grid voltage). (a) Converter currents. (b) Grid currents. (c) Capacitor voltages. (d) Switch positions.

of (6) (with $t = T_1$) becoming

$$\boldsymbol{f} = \sum_{i=0}^{i=N} \int_{t_i^*}^{t_{i+1}^*} \boldsymbol{e}^{\boldsymbol{F}(T_1-\tau)} \mathrm{d}\tau \boldsymbol{G} \boldsymbol{u}_{abc}^*(t_i^*)$$
$$= \boldsymbol{F}^{-1} \sum_{i=0}^{i=N} \left((\boldsymbol{e}^{\boldsymbol{F}(T_1-t_i^*)} - \boldsymbol{e}^{\boldsymbol{F}(T_1-t_{i+1}^*)}) \boldsymbol{G} \boldsymbol{u}_{abc}^*(t_i^*) \right)$$

where $\boldsymbol{F}$ is assumed to be invertible for convenience.[2] Thus, the steady-state value at the end of the fundamental period is

$$\boldsymbol{x}_{\mathrm{OPP}}^*(T_1) = \boldsymbol{e}^{\boldsymbol{F}T_1} \boldsymbol{x}_{\mathrm{OPP},0}^* + \boldsymbol{f}. \tag{9}$$

It is easy to show from (7) [after inserting (8) and (9)] that the initial steady-state value resulting from the pulse pattern is

$$\boldsymbol{x}_{\mathrm{OPP},0}^* = (\mathbf{I}_{n_x} - \boldsymbol{e}^{\boldsymbol{F}T_1})^{-1} \boldsymbol{f} \tag{10}$$

where $\boldsymbol{x}_{\mathrm{OPP},0}$ is assumed to be unique in the steady state.[3]

With the initial steady-state value $\boldsymbol{x}_{\mathrm{OPP},0}^*$ known, the steady-state trajectory $\boldsymbol{x}_{\mathrm{OPP}}^*$ resulting from the pulse pattern can be calculated over the fundamental period using (6). Typically, the steady-state trajectory $\boldsymbol{x}^*$ is required at discrete sampling instants of T_s (the sampling interval of the controller).

[2]In the case that $\boldsymbol{F}$ is singular, the structure of the matrix must be exploited to solve the integral. For the singular matrix $\boldsymbol{F} = \begin{bmatrix} a & 0 \\ 0 & 0 \end{bmatrix}$, for example, the expression $\int_0^t \boldsymbol{e}^{\boldsymbol{F}t} dt = \begin{bmatrix} (e^{at}-1)/a & 0 \\ 0 & t \end{bmatrix}$ can be derived.

[3]This is true for most plants. However, for plants where the resistive components are not taken into account (such as an integrator or resonator), there is no unique trajectory since $\boldsymbol{e}^{\boldsymbol{F}t}$ will not diminish as $t \to \infty$. If no unique trajectory exists, some components of $\boldsymbol{x}_{\mathrm{OPP},0}^*$ must be treated as free variables.

Now, consider the grid voltage. The steady-state trajectory resulting from the grid voltage can be described as

$$\boldsymbol{x}_g^*(t) = \boldsymbol{e}^{\boldsymbol{F}t} \boldsymbol{x}_{g,0}^* + \int_0^t \boldsymbol{e}^{\boldsymbol{F}(t-\tau)} \boldsymbol{P} \boldsymbol{v}_g(\tau) \mathrm{d}\tau$$

where the integral is not trivial to solve since the grid voltage is sinusoidal. Fortunately, the effect of the grid can be calculated using well-known phasor analysis; all the converter states resulting from the grid voltage only consist of a fundamental component. After calculating the effect of the grid voltage over the fundamental period, the steady-state trajectory resulting from the grid voltage can be added to that of the pulse pattern, as shown with (5). Alternatively, the effect of the grid voltage can be considered by representing the grid voltage as a harmonic resonator and including it as additional state variables. Fig. 3 shows an example of a steady-state trajectory $\boldsymbol{x}^*$ in the abc reference frame. The parameters of the system can be found in [4, Appendix C]. The pulse number is $d = 5$ and the system is operating at rated conditions with unity power factor.

IV. Small-Signal Modeling of Modifications of a Pulse Pattern

This section explains how the modifications of a pulse pattern are modeled.

A. Overview of Small-Signal Modeling

Although no clear definition of *small-signal modeling* could be found in the literature, the term, usually, refers to the linearization of a nonlinear system around an operating point [21, Sec. 3.10]. Note that small-signal modeling does not strictly

imply a linearization around a single operating point; the system can also be linearized around a trajectory (which is the case in this article).

There are three types of variables associated with small-signal modeling. The first are the *complete-signal variables*

$$\xi(t) = \xi^*(t) + \tilde{\xi}(t) \tag{11}$$

which is the sum of the *large-signal variables* ξ^* and *small-signal variables* $\tilde{\xi}$. The large-signal variables represent the trajectory that the system is linearized around. The small-signal quantities $\tilde{\xi}$ represent the linearized variables, which are the perturbations superimposed on the large-signal variables. In this article, the large-signal variables are the steady-state variables (the nominal pulse pattern and its resulting steady-state trajectory), which are interpreted as references. The complete-signal variables represent the actual (measured) values of the system. From (11), the small-signal variables can be expressed as

$$\tilde{\xi}(t) = \xi(t) - \xi^*(t) \tag{12}$$

which is interpreted as an error (specifically, small-signal state variables represent errors). A controller can be used to modify the small-signal input in order to drive the small-signal state variables to zero. In steady-state conditions, all small-signal variables are zero (assuming idealized conditions).

B. Linear Approximation to Modifications of a Pulse Pattern

For the moment, only single-phase pulse patterns are considered for convenience. Before continuing, two types of pulse patterns are introduced. The first is the reference pulse pattern, denoted with u^*, and is referred to as the *nominal pulse pattern*. The nominal pulse pattern has n switching transitions that occur at the *nominal* switching instants $t_i^*, i = 1, \ldots, n$, and can be represented as

$$u^*(t) = u_0 + \sum_{i=1}^{n} \Delta u_i h(t - t_i^*) \tag{13}$$

where h is the Heaviside (unit) step function and u_0 is the initial (nominal) switch position. The direction of a switching transition is denoted by $\Delta u_i = u_i - u_{i-1}$, where $u_{i-1}, u_i \in \mathbb{Z}$. The nominal pulse pattern is the offline-calculated pulse pattern.

The second pulse pattern is called the *modified pulse pattern* and it is denoted with u. The modified pulse pattern has modified switching transitions that occur at the *modified* switching instants

$$t_i = t_i^* + \Delta t_i$$

where Δt_i is the time modification. The modified pulse pattern can be represented as

$$u(t) = u_0 + \sum_{i=1}^{n} \Delta u_i h(t - (t_i^* + \Delta t_i)). \tag{14}$$

It can be observed in Fig. 4 that the ith switching time modification is associated with an area of

$$\lambda_i = -\Delta t_i \Delta u_i \tag{15}$$

that is removed or added to the nominal pulse pattern.

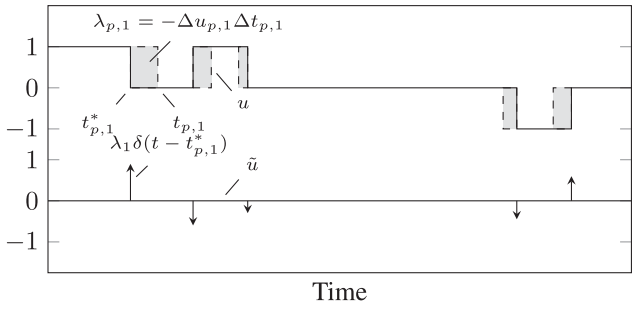

Fig. 4. Using impulses to represent rectangular pulses (that is, modifications to a pulse pattern).

Recall that the time derivative of the step function h is the Dirac delta function, or simply the impulse δ. By using a first-order Taylor series expansion of the step functions around the nominal switching times t_i^*, (14) can be approximated by

$$u(t) \approx u_0 + \sum_{i=1}^{n} \Delta u_i \left(h(t - t_i^*) - \Delta t_i \delta(t - t_i^*)\right)$$

which can be written as[4]

$$u(t) = u_0 + \sum_{i=1}^{n} \Delta u_i h(t - t_i^*) + \sum_{i=1}^{n} \lambda_i \delta(t - t_i^*) \tag{16}$$

with the definition of (15). The (linearized) modified pulse pattern in (16) consists of two terms. The first one is the nominal pulse pattern, whereas the second expression states the (approximated) modifications. These modifications are impulses placed at the nominal switching time instants t_i^* with strengths λ_i.

According to the definition of small-signal variables in (12), the *small-signal input* is defined as

$$\begin{aligned} \tilde{u}(t) &= u(t) - u^*(t) \\ &= \sum_{i=1}^{n} \lambda_i \delta(t - t_i^*). \end{aligned} \tag{17}$$

By rewriting (15), the impulse strengths can be translated into the switching time modifications as

$$\Delta t_i = -\frac{\lambda_i}{\Delta u_i}. \tag{18}$$

Note that the translation from impulse strengths to switching time modification is based on the linearization in (16). More specifically, the areas of the (shaded) rectangular pulses in Fig. 4 are *approximated* by the strengths of the impulses; the narrower the rectangular pulses, the better the approximation.

C. Three-Phase Case

This section generalizes the notation and techniques developed in the previous section to the three-phase case. The modification of the ith switching instant of phase $p \in \{a, b, c\}$ is

$$\Delta t_{p,i} = t_{p,i} - t_{p,i}^* \tag{19}$$

[4]For convenience, the approximation is replaced with an equality in the sequel.

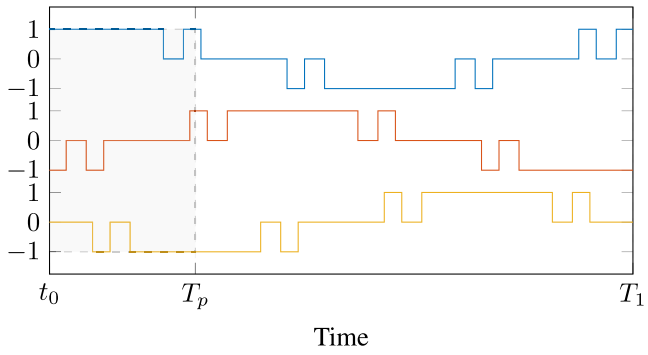

Fig. 5. Three-phase pulse pattern.

where $t_{p,i}$ and $t^*_{p,i}$ are the modified and nominal switching instants, respectively. The (direction of the) ith switching transition in a particular phase is

$$\Delta u_{p,i} = u_{p,i} - u_{p,i-1} \tag{20}$$

where $u_{p,i}, u_{p,i-1} \in \{-1, 0, 1\}$. Generalizing (15), the ith impulse strength in phase p is

$$\lambda_{p,i} = -\Delta t_{p,i} \Delta u_{p,i}. \tag{21}$$

Consider the modified three-phase pulse pattern $\boldsymbol{u}_{abc}$ over the time interval $t \in [0, T_p]$, where T_p is the *prediction horizon* of a predictive controller. Following the principle derived in (16), define the modified pulse pattern as the superposition

$$\boldsymbol{u}_{abc}(t, \lambda_{p,i}) = \boldsymbol{u}^*_{abc}(t) + \tilde{\boldsymbol{u}}_{abc}(t, \lambda_{p,i}) \tag{22}$$

of the three-phase nominal pulse pattern

$$\boldsymbol{u}^*_{abc}(t) = \begin{bmatrix} u_a(t) \\ u_b(t) \\ u_c(t) \end{bmatrix} = \begin{bmatrix} u_{a,0} + \sum_{i=1}^{n_a} \Delta u_{a,i} h(t - t^*_{a,i}) \\ u_{b,0} + \sum_{i=1}^{n_b} \Delta u_{b,i} h(t - t^*_{b,i}) \\ u_{c,0} + \sum_{i=1}^{n_c} \Delta u_{c,i} h(t - t^*_{c,i}) \end{bmatrix} \tag{23}$$

and the three-phase small-signal input

$$\tilde{\boldsymbol{u}}_{abc}(t, \lambda_{p,i}) = \begin{bmatrix} \tilde{u}_a(t, \lambda_{a,i}) \\ \tilde{u}_b(t, \lambda_{b,i}) \\ \tilde{u}_c(t, \lambda_{c,i}) \end{bmatrix} = \begin{bmatrix} \sum_{i=1}^{n_a} \delta(t - t^*_{a,i}) \lambda_{a,i} \\ \sum_{i=1}^{n_b} \delta(t - t^*_{b,i}) \lambda_{b,i} \\ \sum_{i=1}^{n_c} \delta(t - t^*_{c,i}) \lambda_{c,i} \end{bmatrix}. \tag{24}$$

In here, n_p is introduced as the number of switching transitions in phase p that fall within the horizon T_p, and $\lambda_{p,i}$ as the strength of the ith impulse in that phase. Note that the nominal switching times $t^*_{p,i}$ are defined relative to the current time step $t_0 = 0$. The total number of switching transitions in the three phases within the horizon T_p is denoted by $n_{\text{sw}} = n_a + n_b + n_c$. In Fig. 5 , for example, there are $n_{\text{sw}} = 9$ switching transitions ($n_a = 2$, $n_b = 4$, and $n_c = 3$).

V. Small-Signal Controller

This section introduces the generalized model predictive pulse pattern controller, which is referred to as the *small-signal controller*. In the first step, as with any model predictive controller, an internal dynamic model is first derived.

A. Internal Dynamic Model

Recall the differential equation of the power converter system in (3). By integrating (3), and with the modified pulse pattern $\boldsymbol{u}_{abc}$ as the input, the future state vector at time $t \in [0, T_p]$ is

$$\boldsymbol{x}(t, \lambda_{p,i}) = \boldsymbol{e}^{\boldsymbol{F}t} \boldsymbol{x}_0 + \int_0^t \boldsymbol{e}^{\boldsymbol{F}(t-\tau)} \boldsymbol{G} \boldsymbol{u}_{abc}(\tau, \lambda_{p,i}) d\tau + \int_0^t \boldsymbol{e}^{\boldsymbol{F}(t-\tau)} \boldsymbol{P} \boldsymbol{v}_g(\tau) d\tau \tag{25}$$

where $\boldsymbol{x}_0$ is the initial state at time $t_0 = 0$. Similarly, as shown in Section III-C, the (optimal) steady-state trajectory follows from the nominal pulse pattern over the prediction horizon T_p as

$$\boldsymbol{x}^*(t) = \boldsymbol{e}^{\boldsymbol{F}t} \boldsymbol{x}^*_0 + \int_0^t \boldsymbol{e}^{\boldsymbol{F}(t-\tau)} \boldsymbol{G} \boldsymbol{u}^*_{abc}(\tau) d\tau + \int_0^t \boldsymbol{e}^{\boldsymbol{F}(t-\tau)} \boldsymbol{P} \boldsymbol{v}_g(\tau) d\tau \tag{26}$$

where $\boldsymbol{x}^*_0$ is the initial optimal state.[5]

According to (12), the small-signal state vector is defined as

$$\tilde{\boldsymbol{x}}(t, \lambda_{p,i}) = \boldsymbol{x}(t, \lambda_{p,i}) - \boldsymbol{x}^*(t) \tag{27}$$

which is referred to as the *small-signal error*; this term is used to emphasize that the small-signal state vector represents an error. By inserting (26) and (25) with (22) into (27), the small-signal error follows as

$$\tilde{\boldsymbol{x}}(t, \lambda_{p,i}) = \boldsymbol{e}^{\boldsymbol{F}t} \tilde{\boldsymbol{x}}_0 + \int_0^t \boldsymbol{e}^{\boldsymbol{F}(t-\tau)} \boldsymbol{G} \tilde{\boldsymbol{u}}_{abc}(\tau, \lambda_{p,i}) d\tau \tag{28}$$

where $\tilde{\boldsymbol{x}}_0 = \boldsymbol{x}_0 - \boldsymbol{x}^*_0$ is the initial small-signal error. It can be observed that the grid is not a part of the small-signal model. However, the grid voltage is required when selecting the appropriate pulse pattern according to the operating conditions.

In the case of $\boldsymbol{F} = \boldsymbol{0}_{n_x \times n_x}$ (i.e., the system is a pure integrator) and $t = T_p$, it can easily be verified that the internal dynamic model of (28) reduces to that of MP^{3}C in (1). In other words, the proposed controller is a generalization of MP^{3}C to higher-order systems.

B. Compact Vector Form of the Small-Signal Error

The small-signal error (28) can be written in a compact form. First, the small-signal input $\tilde{\boldsymbol{u}}_{abc}$ [see (24)] is decomposed into each phase, resulting in (28) becoming

$$\tilde{\boldsymbol{x}}(t, \lambda_{p,i}) = \boldsymbol{e}^{\boldsymbol{F}t} \tilde{\boldsymbol{x}}_0 + \int_0^t \boldsymbol{e}^{\boldsymbol{F}(t-\tau)} \left(\boldsymbol{G}_a \sum_{i=1}^{n_a} \delta(\tau - t^*_{a,i}) \lambda_{a,i} + \boldsymbol{G}_b \sum_{i=1}^{n_b} \delta(\tau - t^*_{b,i}) \lambda_{b,i} + \boldsymbol{G}_c \sum_{i=1}^{n_c} \delta(\tau - t^*_{c,i}) \lambda_{c,i} \right) d\tau \tag{29}$$

[5]Note that $\boldsymbol{x}^*_0$ of (26) refers to the initial state at the current time instant, whereas $\boldsymbol{x}^*_0$ of (4) refers to the initial state at the start of the fundamental period.

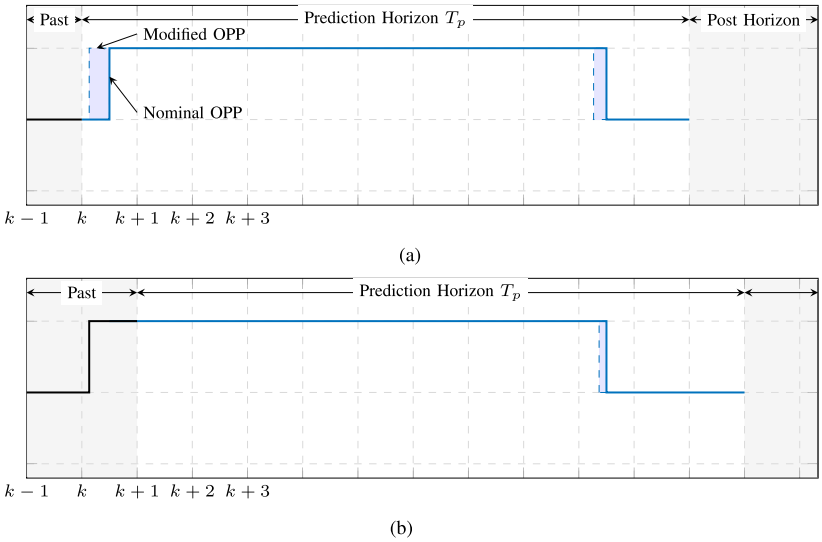

Fig. 6. Receding horizon policy. (a) Prediction horizon at the first sampling instant. (b) Prediction horizon at the second sampling instant.

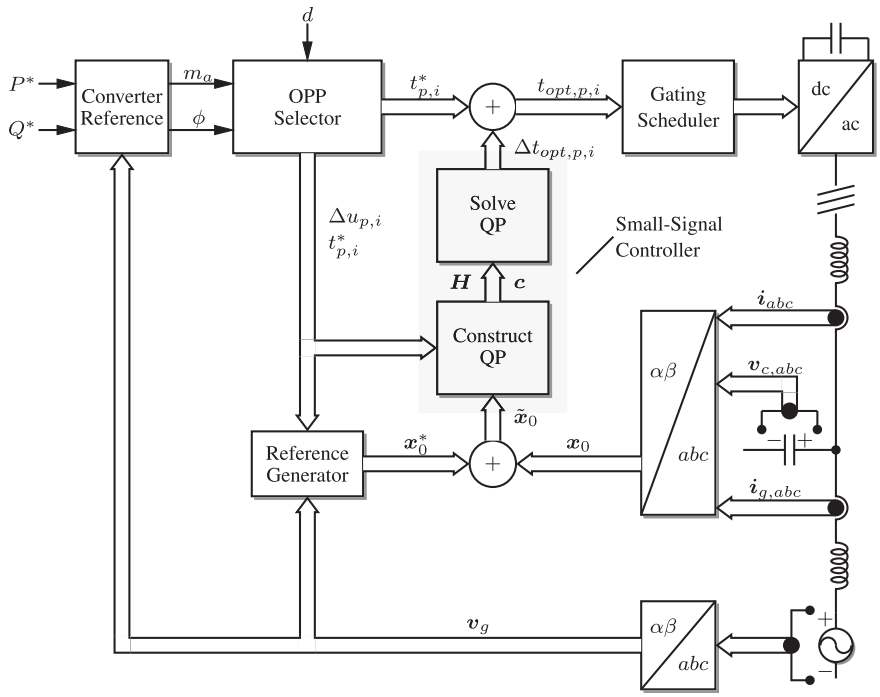

Fig. 7. Block diagram with the small-signal controller.

where $\boldsymbol{G}_a = \boldsymbol{G}[1\,0\,0]^{\mathrm{T}}$, $\boldsymbol{G}_b = \boldsymbol{G}[0\,1\,0]^{\mathrm{T}}$, and $\boldsymbol{G}_c = \boldsymbol{G}[0\,0\,1]^{\mathrm{T}}$. By using the well-known sifting property of the impulse

$$\int_{-\infty}^{t} f(\tau)\delta(\tau - t^*_{p,i})d\tau = f(t^*_{p,i})h(t - t^*_{p,i})$$

and using basic algebraic manipulations, (29) becomes

$$\tilde{\boldsymbol{x}}(t, \boldsymbol{\Lambda}) = \boldsymbol{e}^{\boldsymbol{F}t}\tilde{\boldsymbol{x}}_0 + \boldsymbol{\Phi}(t)\boldsymbol{\Lambda} \tag{30}$$

where $\boldsymbol{\Phi} \in \mathbb{R}^{n_x \times n_{sw}}$ is the input matrix

$$\begin{aligned}\boldsymbol{\Phi}(t) = \Big[&\boldsymbol{e}^{\boldsymbol{F}(t-t^*_{a,1})}\boldsymbol{G}_a h(t - t^*_{a,1}) \cdots \boldsymbol{e}^{\boldsymbol{F}(t-t^*_{a,n_a})}\boldsymbol{G}_a h(t - t^*_{a,n_a}) \\ &\boldsymbol{e}^{\boldsymbol{F}(t-t^*_{b,1})}\boldsymbol{G}_b h(t - t^*_{b,1}) \cdots \boldsymbol{e}^{\boldsymbol{F}(t-t^*_{b,n_b})}\boldsymbol{G}_b h(t - t^*_{b,n_b}) \\ &\boldsymbol{e}^{\boldsymbol{F}(t-t^*_{c,1})}\boldsymbol{G}_c h(t - t^*_{c,1}) \cdots \boldsymbol{e}^{\boldsymbol{F}(t-t^*_{c,n_c})}\boldsymbol{G}_c h(t - t^*_{c,n_c})\Big]\end{aligned} \tag{31}$$

and $\boldsymbol{\Lambda} \in \mathbb{R}^{n_{\text{sw}}}$ is introduced as the *strength vector*

$$\boldsymbol{\Lambda} = [\lambda_{a,1} \ \cdots \ \lambda_{a,n_a} \ \lambda_{b,1} \ \cdots \ \lambda_{b,n_b} \ \lambda_{c,1} \ \cdots \ \lambda_{c,n_c}]^{\mathrm{T}} \tag{32}$$

with the n_{sw} impulse strengths over the horizon T_p. As an example, the strength vector corresponding to Fig. 5 is $\boldsymbol{\Lambda} = [\lambda_{a,1} \ \lambda_{a,2} \ \lambda_{b,1} \ \lambda_{b,2} \ \lambda_{b,3} \ \lambda_{b,4} \ \lambda_{c,1} \ \lambda_{c,2} \ \lambda_{c,3}]^{\mathrm{T}}$.

C. Objective Function

The control objectives are to minimize the small-signal error (which relates to the tracking error) across the prediction horizon and to penalize modifications to the nominal pulse pattern (which relates to the control effort). These control objectives can be mapped into a quadratic objective function as[6]

$$J(\boldsymbol{\Lambda}) = \int_0^{T_p} \tfrac{1}{2}\|\tilde{\boldsymbol{x}}(t,\boldsymbol{\Lambda})\|_{\boldsymbol{Q}}^2 dt + \tfrac{1}{2}\|\boldsymbol{\Lambda}\|_{\boldsymbol{R}}^2. \tag{33}$$

The first term penalizes with the positive (semi) definite diagonal (penalty) matrix $\boldsymbol{Q} \in \mathbb{R}^{n_x \times n_x}$, the integral of the small-signal error over the prediction horizon T_p. The diagonal (penalty) matrix $\boldsymbol{R} \in \mathbb{R}^{n_{\text{sw}} \times n_{\text{sw}}}$ corresponding to the penalty on the switching modifications is also required to be positive (semi) definite. The penalty on the control effort inhibits the controller being overly aggressive. This is useful when modeling errors (recall that the modifications to a pulse pattern are approximated and not exact) and noise (from measurement devices and observers) are present in a system.

The objective function can be written as the quadratic function

$$J(\boldsymbol{\Lambda}) = \tfrac{1}{2}\boldsymbol{\Lambda}^{\mathrm{T}}\boldsymbol{H}\boldsymbol{\Lambda} + \boldsymbol{c}^{\mathrm{T}}\boldsymbol{\Lambda} \tag{34}$$

where $\boldsymbol{H} \in \mathbb{R}^{n_{\text{sw}} \times n_{\text{sw}}}$ is known as the *Hessian* and contains the second-order partial derivatives of J, and $\boldsymbol{c} \in \mathbb{R}^{n_{\text{sw}}}$ is a vector with linear coefficients. The derivation of (34) can be found in Appendix B.

D. Constraints

Constraints are required on the switching time modifications to ensure a feasible pulse pattern. Specifically, the modified switching transitions of each phase are required to be in ascending order, nonnegative, and not moved beyond the prediction horizon, that is

$$0 \le t_{p,1} \le t_{p,2} \le \cdots \le t_{p,n_p} \le T_p \tag{35}$$

for all $p \in \{a,b,c\}$. Alternatively, the n_pth switching transition in a phase can be upper bounded by the next nominal switching transition beyond the horizon, t^*_{p,n_p+1}. Since the impulse strengths $\lambda_{p,i}$ are the decision variables, the set of constraints (35) can be recast in terms of the impulse strengths $\lambda_{p,i}$ with the help of (19) and (21) as

$$0 \le t^*_{p,1} - \frac{\lambda_{p,1}}{\Delta u_{p,1}} \le \ldots \le t^*_{p,n_p} \frac{\lambda_{p,n_p}}{\Delta u_{p,n_p}} \le T_p. \tag{36}$$

[6]The scaling factor of $\frac{1}{2}$ is added to ensure the problem can be written in the standard quadratic form.

Applying (36) to the phases a, b, and c, the constraint

$$\boldsymbol{A}\boldsymbol{\Lambda} \le \boldsymbol{b} \tag{37}$$

in the matrix form arises, with $\boldsymbol{A} = \text{blockdiag}(\boldsymbol{A}_a, \boldsymbol{A}_b, \boldsymbol{A}_c) \in \mathbb{R}^{(n_{\text{sw}}+3)\times n_{\text{sw}}}$ and $\boldsymbol{b} = [\boldsymbol{b}_a^{\mathrm{T}} \ \boldsymbol{b}_b^{\mathrm{T}} \ \boldsymbol{b}_c^{\mathrm{T}}]^{\mathrm{T}} \in \mathbb{R}^{n_{\text{sw}}+3}$, where $\boldsymbol{A}_p$ and $\boldsymbol{b}_p$ are defined in Appendix C.

E. Quadratic Program

Minimizing the objective function (34) while respecting the constraint (37) leads to the QP

$$\boldsymbol{\Lambda}_{\text{opt}} = \arg\min_{\boldsymbol{\Lambda}} \quad \frac{1}{2}\boldsymbol{\Lambda}^{\mathrm{T}}\boldsymbol{H}\boldsymbol{\Lambda} + \boldsymbol{c}^{\mathrm{T}}\boldsymbol{\Lambda} \tag{38a}$$

$$\text{subject to} \quad \boldsymbol{A}\boldsymbol{\Lambda} \le \boldsymbol{b}. \tag{38b}$$

The strength vector $\boldsymbol{\Lambda}$ in (32) is the decision (or optimization) variable, and $\boldsymbol{\Lambda}_{\text{opt}}$ is the optimal solution to the QP. The latter cannot be computed algebraically; instead, numerical optimization techniques must be employed, such as gradient methods, active-set methods, or interior point methods.

Note that the problem (38) is convex, since the constraints are linear and the objective function is quadratic in the decision variable with a positive (semi) definite Hessian $\boldsymbol{H}$. This can be shown from the fact that the penalty matrices $\boldsymbol{Q}$ and $\boldsymbol{R}$ are positive (semi) definite.

F. Optimal Switching Instants

Having solved the QP (38), the vector of the optimal impulse strengths $\boldsymbol{\Lambda}_{\text{opt}}$ is translated with (21) into the optimal switching instant modifications

$$\Delta t_{\text{opt},p,i} = -\frac{\lambda_{\text{opt},p,i}}{\Delta u_{p,i}}. \tag{39}$$

By adding these modifications to the nominal switching instants of the pulse pattern, the optimal switching instants are obtained as

$$t_{\text{opt},p,i} = t^*_{p,i} - \frac{\lambda_{\text{opt},p,i}}{\Delta u_{p,i}} \tag{40}$$

where (19) has been rewritten.

G. Receding Horizon Policy

The controller operates at discrete-time steps kT_s, where $k \in \mathbb{N}$, and T_s is the sampling interval. Note that even though the controller operates at discrete-time instants kT_s, the switching instant modification is formulated in the continuous-time domain. This implies that the modified switching instants are real-valued quantities.

Out of the long prediction horizon, only the modified switching instants within the current sampling interval are applied, that is, between kT_s and $(k+1)T_s$. Then, at each subsequent sampling instant, the modified switching instants from the previous sampling instant are discarded and the nominal switching instants are reoptimized based on new information. This process, illustrated in Fig. 6, is known as the *receding horizon* policy [22, Sec. 1.1], which provides feedback

and makes the controller robust to disturbances and modeling errors.

H. Summary

The overall control diagram, with the small-signal controller included, is shown in Fig. 7. The control algorithm consists of the following steps.

1) The real power P^* and reactive power Q^* references are mapped into a modulation index m_a and pulse pattern phase ϕ, which depends on the grid voltage $\boldsymbol{v}_g$ in the *converter reference* block via simple phasor analysis.
2) For the given modulation index m_a and the selected pulse number d, the nominal pulse pattern is read-out from a lookup table and phase-shifted accordingly by ϕ in the *OPP selector* block.
3) The optimal state reference trajectory $\boldsymbol{x}^*$ is generated over a fundamental period in the block *reference generator*, as explained in Section III-C.
4) At a given sampling instant, the *reference generator* supplies the initial (reference) state $\boldsymbol{x}_0^*$.
5) The small-signal controller first calculates the initial small-signal error, $\tilde{\boldsymbol{x}}_0 = \boldsymbol{x}_0 - \boldsymbol{x}_0^*$. Then, in the block *construct QP*, it builds the Hessian $\boldsymbol{H}$ according to (45) and the coefficient vector $\boldsymbol{c}$ according to (48) in Appendix B.
6) By solving the QP (38) in the *solve QP* block, the vector of optimal impulse strengths $\boldsymbol{\Lambda}_{\text{opt}}$ is found. The strengths $\lambda_{p,i}$ are translated back to the transition advancements and delays $\Delta t_{\text{opt},p,i}$, which are then added to the nominal switching times $t_{p,i}^*$ of the pulse pattern to yield the optimal (modified) switching instants $t_{\text{opt},p,i}$, in accordance with (40).
7) The switching transitions within the sampling interval are applied by the *gating scheduler* block.

Note that the Steps 1–3 are only required if the operating point changes.

VI. Conclusion

The original MP^{3}C concept in [9] was devised for first-order systems, such as the stator winding of an electrical machine. This article generalized MP^{3}C to make it applicable to higher-order systems, such as grid-connected converters with an LC filter. The switching instant modifications of the pulse pattern are modified by the controller to regulate the state vector along its optimal trajectory. Assuming that these corrections occur instantaneously at the nominal switching instants allows one to model the corrections as strengths of impulses. This simplification ensures that the state dynamics are linear in the controller corrections; the resulting optimization problem underlying the model predictive controller is, thus, a QP.

The second part of this article will show how the control algorithm can be implemented on a low-cost field-programmable gate array and how it is able to execute in real-time within a short sampling interval [4].

Appendix A
State-Space Matrices

The state-space matrices of the case study are

$$\boldsymbol{F} = \begin{bmatrix} -\frac{R+R_C}{L}\mathbf{I}_2 & \frac{R_C}{L}\mathbf{I}_2 & -\frac{1}{L}\mathbf{I}_2 \\ \frac{R_C}{L_{gt}}\mathbf{I}_2 & -\frac{R_{gt}+R_C}{L_{gt}}\mathbf{I}_2 & \frac{1}{L_{gt}}\mathbf{I}_2 \\ \frac{1}{C}\mathbf{I}_2 & -\frac{1}{C}\mathbf{I}_2 & \mathbf{0}_{2\times 2} \end{bmatrix}$$

$$\boldsymbol{G} = \frac{V_d}{2L}\begin{bmatrix} \mathbf{I}_2 \\ \mathbf{0}_{2\times 2} \\ \mathbf{0}_{2\times 2} \end{bmatrix}\boldsymbol{K}, \text{ and } \boldsymbol{P} = \frac{1}{L_{gt}}\begin{bmatrix} \mathbf{0}_{2\times 2} \\ -\mathbf{I}_2 \\ \mathbf{0}_{2\times 2} \end{bmatrix}.$$

In here, $\mathbf{I}_2$ denotes the identity matrix with dimensions two, and $\mathbf{0}_{2\times 2}$ is a 2×2 zero matrix.

Appendix B
Derivation of the Quadratic Form

Consider the two terms of the objective function, see (33). The first term can be expanded to

$$\begin{aligned} J_1(\boldsymbol{\Lambda}) &= \tfrac{1}{2}\int_0^{T_p} \left(\boldsymbol{e}^{\boldsymbol{F}t}\tilde{\boldsymbol{x}}_0 + \boldsymbol{\Phi}(t)\boldsymbol{\Lambda}\right)^{\mathrm{T}} \boldsymbol{Q}\left(\boldsymbol{e}^{\boldsymbol{F}t}\tilde{\boldsymbol{x}}_0 + \boldsymbol{\Phi}(t)\boldsymbol{\Lambda}\right) dt \\ &= \tfrac{1}{2}\int_0^{T_p} \left(\boldsymbol{\Lambda}^{\mathrm{T}}\boldsymbol{\Upsilon}(t)\boldsymbol{\Lambda} + \boldsymbol{\Theta}^{\mathrm{T}}(t)\boldsymbol{\Lambda}\right) dt + \theta \\ &= \tfrac{1}{2}\boldsymbol{\Lambda}^{\mathrm{T}}\left(\underbrace{\int_0^{T_p}\boldsymbol{\Upsilon}(t)dt}_{\boldsymbol{V}}\right)\boldsymbol{\Lambda} + \left(\underbrace{\int_0^{T_p}\boldsymbol{\Theta}^{\mathrm{T}}(t)dt}_{\boldsymbol{c}}\right)\boldsymbol{\Lambda} + \theta \end{aligned} \tag{41}$$

where

$$\boldsymbol{\Upsilon}(t) = \boldsymbol{\Phi}^{\mathrm{T}}(t)\boldsymbol{Q}\boldsymbol{\Phi}(t) \tag{42}$$

$$\boldsymbol{\Theta}^{\mathrm{T}}(t) = (\boldsymbol{e}^{\boldsymbol{F}t}\tilde{\boldsymbol{x}}_0)^{\mathrm{T}}\boldsymbol{Q}\boldsymbol{\Phi}(t) \tag{43}$$

and

$$\theta = \tfrac{1}{2}\int_0^{T_p} (\boldsymbol{e}^{\boldsymbol{F}t}\tilde{\boldsymbol{x}}_0)^{\mathrm{T}}\boldsymbol{Q}(\boldsymbol{e}^{\boldsymbol{F}t}\tilde{\boldsymbol{x}}_0)\, dt. \tag{44}$$

Consider the $(i,' j')$th entry of the $n_{\text{sw}} \times n_{\text{sw}}$ matrix $\boldsymbol{V}$ [i.e., the integral of (42)]. Assume that the i'th entry corresponds to phase $p_1 \in \{a, b, c\}$ and the ith switching transition in that phase. Using Fig. 5 as an example, $i' = 5$ refers to $p_1 = b$ and $i = 3$. The quantities p_2 and j are defined accordingly for a given j'. Following some algebraic manipulations, it can be shown that the $(i,' j')$th entry of $\boldsymbol{V}$ is

$$\boldsymbol{V}_{(i,'j')} = \boldsymbol{G}_{p_1}^{\mathrm{T}} e^{\boldsymbol{F}^{\mathrm{T}}(t_{ij}^* - t_{p_1,i}^*)}\boldsymbol{\Xi}(T_p - t_{ij}^*)e^{\boldsymbol{F}(t_{ij}^* - t_{p_2,j}^*)}\boldsymbol{G}_{p_2} \tag{45}$$

where $t_{ij}^* = \max\{t_{p_1,i}^*, t_{p_2,j}^*\}$, and

$$\boldsymbol{\Xi}(\Delta t) = \int_0^{\Delta t} \boldsymbol{e}^{\boldsymbol{F}^{\mathrm{T}}\tau}\boldsymbol{Q}\boldsymbol{e}^{\boldsymbol{F}\tau} d\tau. \tag{46}$$

Calculating the integral of the product of two matrix exponentials, which do not commute, is not trivial. Recall the following

theorem from [23]: The integral of (46) can be calculated as

$$\boldsymbol{\Xi}(\Delta t) = \boldsymbol{M}^{\mathrm{T}}(\Delta t)\boldsymbol{N}(\Delta t) \tag{47}$$

where

$$e^{\begin{bmatrix} -\boldsymbol{F}^{\mathrm{T}} & \boldsymbol{Q} \\ \boldsymbol{0}_{n_x \times n_x} & \boldsymbol{F} \end{bmatrix} \Delta t} = \begin{bmatrix} & \overbrace{\qquad\qquad\qquad\qquad} \boldsymbol{N}(\Delta t) \\ e^{-\boldsymbol{F}^{\mathrm{T}}\Delta t} & e^{-\boldsymbol{F}^{\mathrm{T}}\Delta t}\int_0^{\Delta t} e^{\boldsymbol{F}^{\mathrm{T}}\tau}\boldsymbol{Q}e^{\boldsymbol{F}\tau}d\tau \\ \boldsymbol{0}_{n_x \times n_x} & \underbrace{e^{\boldsymbol{F}\Delta t}}_{\boldsymbol{M}(\Delta t)} \end{bmatrix}.$$

Following similar derivations, it can be shown that i'th entry of the n_{sw}-dimensional column vector $\boldsymbol{c}$ [i.e., the integral of (43)] is

$$\boldsymbol{c}_{i'}^{\mathrm{T}} = \tilde{\boldsymbol{x}}_0^{\mathrm{T}} e^{\boldsymbol{F}^{\mathrm{T}} t^*_{p,i}} \boldsymbol{\Xi}(T_p - t^*_{p,i})\boldsymbol{G}_p. \tag{48}$$

Note that θ in (41) is not a function of the strength vector $\boldsymbol{\Lambda}$. Therefore, it is merely a constant in the objective function, which has no influence on the solution of the to-be-derived optimization problem. This fact allows θ to be omitted hereafter.

The first term of the objective function, J_1, which minimizes the small-signal error, can now be written as

$$J_1(\boldsymbol{\Lambda}) = \frac{1}{2}\boldsymbol{\Lambda}^{\mathrm{T}}\boldsymbol{V}\boldsymbol{\Lambda} + \boldsymbol{c}^{\mathrm{T}}\boldsymbol{\Lambda}. \tag{49}$$

The second term of the objective function (33), which penalizes the entries of the strength vector $\boldsymbol{\Lambda}$, is simply

$$J_2(\boldsymbol{\Lambda}) = \frac{1}{2}\boldsymbol{\Lambda}^{\mathrm{T}}\boldsymbol{R}\boldsymbol{\Lambda}. \tag{50}$$

The objective function can now be written in its standard quadratic form as

$$\begin{aligned} J(\boldsymbol{\Lambda}) = J_1(\boldsymbol{\Lambda}) + J_2(\boldsymbol{\Lambda}) &= \frac{1}{2}\boldsymbol{\Lambda}^{\mathrm{T}}(\boldsymbol{V}+\boldsymbol{R})\boldsymbol{\Lambda} + \boldsymbol{c}^{\mathrm{T}}\boldsymbol{\Lambda} \\ &= \frac{1}{2}\boldsymbol{\Lambda}^{\mathrm{T}}\boldsymbol{H}\boldsymbol{\Lambda} + \boldsymbol{c}^{\mathrm{T}}\boldsymbol{\Lambda}. \end{aligned} \tag{51}$$

APPENDIX C
MATRIX FORM OF CONSTRAINTS

The matrix $\boldsymbol{A}_p \in \mathbb{R}^{(n_p+1)\times n_p}$ and vector $\boldsymbol{b}_p \in \mathbb{R}^{n_p+1}$ are defined as

$$\boldsymbol{A}_p = \begin{bmatrix} \frac{1}{\Delta u_{p,1}} & 0 & 0 & \cdots & 0 & 0 \\ -\frac{1}{\Delta u_{p,1}} & \frac{1}{\Delta u_{p,2}} & 0 & \cdots & 0 & 0 \\ 0 & -\frac{1}{\Delta u_{p,2}} & \frac{1}{\Delta u_{p,3}} & \cdots & 0 & 0 \\ \vdots & & & \ddots & \vdots & \vdots \\ 0 & 0 & 0 & \cdots & -\frac{1}{\Delta u_{p,n_p-1}} & \frac{1}{\Delta u_{p,n_p}} \\ 0 & 0 & 0 & \cdots & 0 & \frac{1}{\Delta u_{p,n_p}} \end{bmatrix}$$

and

$$\boldsymbol{b}_p = \begin{bmatrix} t^*_{p,1} & t^*_{p,2} - t^*_{p,1} & \cdots & T_p - t^*_{p,n_p} \end{bmatrix}^{\mathrm{T}}$$

respectively.

ACKNOWLEDGMENT

Tinus Dorfling would like to thank ABB System Drives for their financial support.

REFERENCES

[1] G. S. Buja and G. B. Indri, "Optimal pulsewidth modulation for feeding AC motors," *IEEE Trans. Ind. Appl.*, vol. IA-13, no. 1, pp. 38–44, Jan. 1977.
[2] J. Scoltock, T. Geyer, and U. K. Madawala, "A comparison of model predictive control schemes for MV induction motor drives," *IEEE Trans. Ind. Informat.*, vol. 9, no. 2, pp. 909–919, May 2013.
[3] T. Geyer, *Model Predictive Control of High Power Converters and Industrial Drives*. Chichester, U.K.: Wiley, Nov. 2016.
[4] T. Dorfling, H. d. T. Mouton, and T. Geyer, "Generalized model predictive pulse pattern control based on small-signal modelling—Part 2: Implementation and analysis," *IEEE Trans. Power Electron.*, to be published, doi: 10.1109/TPEL.2022.3169119.
[5] J. Holtz and B. Beyer, "Off-line optimized synchronous pulsewidth modulation with on-line control during transients," *Eur. Power Electron. Drives J.*, vol. 1, pp. 193–200, Jan. 1991.
[6] J. Holtz and N. Oikonomou, "Synchronous optimal pulsewidth modulation and stator flux trajectory control for medium-voltage drives," *IEEE Trans. Ind. Appl.*, vol. 43, no. 2, pp. 600–608, Mar./Apr. 2007.
[7] J. Holtz and N. Oikonomou, "Estimation of the fundamental current in low-switching-frequency high dynamic medium-voltage drives," *IEEE Trans. Ind. Appl.*, vol. 44, no. 5, pp. 1597–1605, Sep./Oct. 2008.
[8] M. Morari and J. H. Lee, "Model predictive control: Past, present and future," *Comput. Chem. Eng.*, vol. 23, pp. 667–682, May 1999.
[9] T. Geyer, N. Oikonomou, G. Papafotiou, and F. D. Kieferndorf, "Model predictive pulse pattern control," *IEEE Trans. Ind. Appl.*, vol. 48, no. 2, pp. 663–676, Mar.–Apr. 2012.
[10] ABB, "Industrial drive, ACS6080," Accessed: May 5, 2021. [Online]. Available: https://new.abb.com/drives/medium-voltage-ac-drives/acs6080
[11] T. Geyer and V. Spudic, "Carrier-based model predictive pulse pattern control," in *Proc. IEEE Energy Convers. Congr. Expo.*, 2018, pp. 4024–4031.
[12] A. Hoffmann, M. Wagner, and S. Bernet, "A novel control scheme for medium voltage drives operated by optimized pulse patterns," in *Proc. IEEE Energy Convers. Congr. Expo.*, Montreal, QC, Canada, Sep. 2015, pp. 4488–4495.
[13] I. Pejcic, "Spectral predictive control in power electronics," M.S. thesis, Elect. Electron. Eng., Swiss Federal Inst. Technol. Lausanne, Lausanne, Switzerland, Aug. 2014.
[14] P. Hokayem, T. Geyer, and N. Oikonomou, "Active damping for model predictive pulse pattern control," in *Proc. IEEE Energy Convers. Congr. Expo.*, 2014, pp. 1220–1227.
[15] I. Pejcic, S. Almer, and H. Peyrl, "Voltage source converter MPC with optimized pulse patterns and minimization of integrated squared tracking error," in *Proc. Amer. Control Conf.,*2017, pp. 4069–4074.
[16] S. Almer, "Predictive pulse pattern control of an inverter with LCL filter: A nonlinear transformation approach," in *Proc. IEEE 3rd Int. Future Energy Electron. Conf. ECCE Asia*, 2017, pp. 1031–1036.
[17] A. Birth, "Model predictive control of a medium-voltage grid-connected converter with LC filter using optimal pulse patterns with relaxed symmetry," M.S. thesis, Fac. Eng., Stellenbosch Univ., Stellenbosch, South Africa, 2020.
[18] J. Holtz and N. Oikonomou, "Neutral point potential balancing algorithm at low modulation index for three-level inverter medium-voltage drives," *IEEE Trans. Ind. Appl.*, vol. 43, no. 3, pp. 761–768, May/Jun. 2007.
[19] T. Geyer and V. Spudic, "Model predictive pulse pattern control with integrated balancing of the neutral point potential," in *Proc. 21st Eur. Conf. Power Electron. Appl.*, 2019, pp. P.1–P.10.
[20] T. Mouton and T. Geyer, "Trajectory-based LQR control of a grid-connected converter with an LCL filter," in *Proc. IFAC Conf. Nonlinear Model Predictive Control*, 2018, vol. 51, pp. 273–278.
[21] G. C. Goodwin, S. F. Graebe, and M. E. Salgado, *Control System Design*. Upper Saddle River, NJ, USA: Prentice-Hall, 2001.
[22] L. Grüne and J. Pannek, *Nonlinear model predictive control: Theory and algorithms, Commun. Control Eng.*, 2nd ed., Cham, Switzerland: Springer, 2017.
[23] C. V. Loan, "Computing integrals involving the matrix exponential," *IEEE Trans. Autom. Control*, vol. 23, no. 3, pp. 395–404, Jun. 1978.

Tinus Dorfling received the B.Eng. degree in electrical and electronic engineering and the M.Eng. and Ph.D. degrees in electrical engineering from the University of Stellenbosch, Stellenbosch, South Africa, in 2015, 2018, and 2021, respectively.

In 2021, he joined ABB Corporate Research Centre, Baden-Dättwil, Switzerland, as a Scientist. His research interests include modulation and control techniques for medium-voltage converter systems, with specific interests in optimized pulse patterns, model predictive control, and the implementation of control algorithms on FPGAs.

Hendrik du Toit Mouton (Member, IEEE) received the B.Sc., B.Sc. (Hons.), M.Sc., and Ph.D. degrees in mathematics from the University of the Free State, Bloemfontein, South Africa, in 1986, 1987, 1988, and 1991, respectively, and the B.Eng. and Ph.D. degrees in electrical engineering from the University of Stellenbosch, Stellenbosch, South Africa, in 1996 and 2000, respectively.

He is currently a Professor of electrical engineering with the University of Stellenbosch and the Leader of Power Electronics Research Group. He has authored or coauthored more than 130 journal and conference papers in mathematics and power electronics. His research interests include multilevel converters, modeling and control of power electronic converters, and class-D audio amplifiers.

Tobias Geyer (Fellow, IEEE) received the Dipl.-Ing. degree in electrical engineering, the Ph.D. degree in control engineering, and the Habilitation degree in power electronics from ETH Zurich, Zürich, Switzerland, in 2000, 2005, and 2017, respectively.

After his Ph.D., he spent three years with GE Global Research, Munich, Germany, three years with the University of Auckland, Auckland, New Zealand, and eight years with ABB's Corporate Research Centre, Baden-Dättwil, Switzerland, where his last position was that of a Senior Principal Scientist for power conversion control. In 2020, he joined ABB's Medium-Voltage Drive Division as the R&D Platform Manager of the ACS6080. Working at the intersection of industry and academia, he is also an Extraordinary Professor with Stellenbosch University, Stellenbosch, South Africa. He has authored the book *Model Predictive Control of High Power Converters and Industrial Drives* (Wiley, 2016) and holds 35 patent families. He teaches a regular course on model predictive control at ETH Zurich. His research interests include medium-voltage and low-voltage drives, utility-scale power converters, optimized pulse patterns, and model predictive control.

Dr. Geyer was the recipient of the Semikron Innovation Award and the Nagamori Award, both in 2021, two Prize Paper Awards of IEEE transactions and two Prize Paper Awards at IEEE conferences. From 2011 to 2014, he was an Associate Editor for the TRANSACTIONS ON INDUSTRY APPLICATIONS and from 2013 to 2019, for the TRANSACTIONS ON POWER ELECTRONICS. He was an International Program Committee Vice Chair of the IFAC conference on Nonlinear Model Predictive Control in Madison, WI, USA, in 2018. He is also a Distinguished Lecturer of the Power Electronics Society from the year 2020 until 2023.